Pharm Res (2012) 29:2167–2179
DOI 10.1007/s11095-012-0745-1

RESEARCH PAPER

Galactose Decorated Acid-Labile Nanoparticles Encapsulating Quantum Dots for Enhanced Cellular Uptake and Subcellular Localization

Xiaojun Cai • Xiaohong Li • Yaowen Liu • Guannan Wu • Yuancong Zhao • Fang Chen • Zhongwei Gu

Received: 28 December 2011 / Accepted: 19 March 2012 / Published online: 5 April 2012

ABSTRACT

Purpose Biodegradable polymers containing acid-labile segments and galactose grafts were formulated into nanoparticles in current study, and enhanced cellular uptake and subcellular distribution were clarified.

Methods Quantum dots (QDs) was utilized as an imaging agent and a model of bioactive substances, and entrapped into nanoparticles of around 200 nm through a nanoprecipitation process.

Results The acid-labile characteristics of QDs-loaded nanoparticles were approved by the hemolysis capability, the degradation behaviors of matrix polymers, and the fluorescence decay of entrapped QDs after incubation into buffer solutions of different pH values. The galactose grafts increased the acid-lability, due to the hydrophilic moieties on the acid-labile segments, and enhanced uptake efficiency of over 50 % was found after 4 h incubation with HepG2 cells, due to the galactose-receptor mediated endocytosis. The acid-lability led to an efficient endosomal escape of QDs-loaded nanoparticles into cytoplasm.

Conclusions The integration of acid-lability, targeting effect, and full biodegradable backbone into nanoparticle matrices constitutes a promising platform for intracellular delivery of bioactive substances for disease diagnosis, imaging and treatment.

X. Cai • X. Li (✉) • Y. Liu • G. Wu • Y. Zhao • F. Chen
Key Laboratory of Advanced Technologies of Materials
Ministry of Education of China
School of Materials Science & Engineering
Southwest Jiaotong University
Chengdu 610031, People's Republic of China
e-mail: xhli@swjtu.edu.cn

Z. Gu (✉)
National Engineering Research Center for Biomaterials
Sichuan University
Chengdu 610064, People's Republic of China
e-mail: zwgu@scu.edu.cn

KEY WORDS acid-labile biodegradable polymers · cellular uptake · endosomal escape · galactose decoration · quantum dots-loaded nanoparticles

INTRODUCTION

A wide variety of potential biomolecular therapeutics is well established, such as DNA for gene therapy, oligonucleotides for antisense therapy, as well as peptides or proteins for cancer therapy. Numerous biological barriers have imposed great influence on the interactions with targeting cells, the chemical and physical stabilities of biomolecules in the extracellular space (1). Therefore, the biomolecular therapeutics is intensively dependent on the development of drug delivery and targeting systems. Size-dependent passive targeting and chemical moiety-mediated active targeting have been proposed to minimize the structural degradation and activity loss, and to increase the availability of biotherapeutics at the potential active sites (2). However, when biomolecules or the nanocarriers are taken up by targeted cells via endocytosis, they are often rapidly trafficked from early endosome to late endosome, and eventually to lysosome (3), where they are degraded by acid environment and enzymes (4). So the endo-lysosomal escape becomes a crucial step in the intracellular delivery to organelles, which are the locations for many biotherapeutics to carry out their biological functions. There are pH gradients in the extracellular space and different intracellular compartments, for example, the pH values of extracellular environment and cytoplasm are 7.4, whereas those of lysosome and endosome are 5.0–6.5 (5). Therefore, many strategies have focused on the design of intelligent drug carriers with pH-dependent membrane-disruptive abilities (6).

Synthetic polymers containing acid-labile linkage, such as acetal, diortho ester and hydrazone linkers, have been used

for drug delivery to ensure a fast degradation at mildly acidic environments (7). Garripelli *et al.* connected Pluronic-based multiblock copolymers via acid-labile acetal bonds, which formed gels at body temperature and allowed bioresponsive polymer degradation at an acidic pH (8). Guo *et al.* synthesized poly(ethylene glycol)-diortho ester-distearoyl glycerol conjugate, which had the uniquely fast degradation kinetics at pH 5–6 and the ability to stabilize liposomes in serum (9). Most of the pH-dependent polymers were made form non-biodegradable blocks connected by pH-sensitive linkages, and had a similar shortcoming that could not degrade after the delivery of their therapeutic cargo. To ensure a full biodegradability of the carriers, acid-labile segments containing acetal groups were introduced into biodegradable backbone of poly(DL-lactide) in our previous study, and galactose moieties were further conjugated onto above polymers through click chemistry (10).

Semiconductor quantum dots (QDs) have been widely used for fluorescent labeling in the field of biological and medical research. In comparison with traditional organic dyes, QD probes possess high quantum yields, long-term photostability and broad absorption bands, which make it easy to excite multiple colors with a single excitation source (11). However, QDs are not water soluble and have potential cytotoxicity, which have heavily impeded their biological applications (12). Attempts have been made to achieve biofunctionalized QDs, such as conjugation of small molecules and encapsulation into polymer matrices (13). Pan *et al.* prepared folate-decorated nanoparticles with the load of QDs, and the cytotoxicity of QDs was significantly decreased after encapsulation into nanoparticles (14). However, QDs are used mostly in extracellular imaging, due to the lack of an effective means to successfully deliver QDs into cytoplasm without aggregation. In addition, while the endocytosis of QDs is an easy and spontaneous process, it usually results in sequestration of most QDs in the endosomal compartment, and unavailability for subsequent intracellular assays (15).

In our previous study biodegradable polymers containing acid-labile segments and galactose grafts were used to entrap pDNA polyplexes into microspheres with the size of around 2–3 μm, and promoted transfection efficiency was determined on liver macrophages, the potential antigen presenting cells (10). Nanoparticles constitute a versatile drug delivery system, due to their abilities to overcome physiologic barriers and to achieve efficient tissue distribution and cellular uptake. In the present study galactose decorated acid-labile nanoparticles of around 200 nm were explored with the entrapment of QDs to clarify the enhancement of cellular uptake and subcellular localization. QDs were supposed to act as an imaging agent for the cellular trafficking as well as a model of bioactive substances for disease diagnosis, imaging and treatment. It was aimed to test the hypothesis that nanoparticles could accumulate into endosomal compartment due to the receptor-mediated endocytosis, followed by subsequent release into cytoplasm due to the acid-labile characteristics. The acid-lability of the obtained nanoparticles was clarified through the hemolysis capability, matrix degradation behaviors and fluorescence stability of entrapped QDs after incubation in buffer solutions of different pH values. After the cytotoxicity test to obtain an optimal dose, the uptake efficiency and subcellular location of QDs-loaded nanoparticles with or without acetal groups and galactose decoration were determined on HepG2 cells, using MCF-7 breast cancer cells without asialoglycoprotein receptor as control.

MATERIALS AND METHODS

Materials

Galactose grafted poly(benzaldehyde-polyethylene glycol)-poly(DL-lactide) (PGBELA) was prepared through click reaction of 1-O-2-azidoethyl-*β*-*D*-glactose with acid-labile copolymer poly(4-propargyl-benzaldehyde-poly(ethylene glycol))-poly(DL-lactide) (10). Acetal groups were introduced by reacting PEG with benzaldehyde to obtain poly(benzaldehyde-polyethylene glycol), which was further copolymerized with DL-Lactide to obtain poly(benzaldehyde-poly(ethylene glycol))-poly(D,L-lactide) (PBELA) (16). Copolymers poly(ethylene glycol)-poly(DL-lactide) (PELA) were prepared by bulk ring-opening polymerization of lactide/PEG using stannous chloride as initiator (17). The obtained copolymers PGBELA, PBELA and PELA indicated weight-average molecular weight (M_w) of 24.6, 23.8 and 25.8 kDa, and polydispersity indeces (M_w/M_n) of 1.38, 1.21 and 1.33, respectively. Pluronic® F68 and 3-(4,5-dimethylthiazol-2-yl)-2,5-diphenyltetrazolium bromide (MTT) were purchased from Sigma (St. Louis, MO). All other chemicals were analytical grade and received from Changzheng Regents Company (Chengdu, China) unless otherwise indicated.

Preparation of QDs-Loaded Nanoparticles

CdS QDs was prepared in 1-octadecene with oleic acid as a capping agent following our previous report, and the average size was around 4.0 nm (18). QDs-loaded nanoparticles were prepared by a modified nanoprecipitation technique (19). Typically, 20 mg F68 were dissolved in 100 ml water to form a water phase, and 50 mg PGBELA and 10 μM QDs were dissolved in 5 ml acetone to form an organic phase, which was added dropwise into the water phase. The mixture was stirred for 6 h at room temperature to evaporate the residual organic solvent, and then centrifuged at 15000 rpm for 10 min. The precipitate was freeze-dried to collect QD/PGBELA nanoparticles. Similar procedures

were utilized to prepare QD/PBELA and QD/PELA nanoparticles, and blank PELA, PBELA and PGBELA nanoparticles were prepared without QD addition.

Characterization of QDs-Loaded Nanoparticles

The shape and surface morphology of the nanoparticles obtained were examined by scanning electron microscope (SEM, FEI Quanta200, The Netherlands) and transmission electron microscope (TEM, Hitachi H-600-4, Japan). SEM was quipped with field-emission gun (accelerating voltage of 20 kV) and Robinson detector after 2 min of gold coating to minimize charging effect. A small drop of nanoparticle suspension was placed on a glass copper grid (100 meshes) with carbon films and the excess solution was evaporated under vacuum, followed by staining with citric acid solution before TEM measurement. The particle size, size distribution and Zeta potential of QDs-loaded nanoparticles were measured by Zetasizer Nano ZS system (Malvern, UK). QDs-loaded nanoparticle suspension was diluted with deionized water and ultrasonicated for several minutes before measurement.

The nanoparticle forming efficiency indicated the amount of nanoparticles retrieved compared with that of polymers used for the nanoparticle preparation. The encapsulation efficiency of QDs in nanoparticles was evaluated by atomic absorption spectrometer (AAS, SpectrAA 20FS, Varian, Palo Alto, CA). Around 6 mg QDs-loaded nanoparticles were dissolved in 3.0 ml 6.0 mol/l of nitric acid solution at 60 °C before measurement. The encapsulation efficiency indicated the percentage of QDs encapsulated with respect to the total amount used for the nanoparticle preparation. The loading amount of QDs indicated the amount (in μg) of QDs encapsulated per g of nanoparticles. The existence of galactose residual on QD/PGBELA nanoparticles and the incorporation of CdS QDs within nanoparticles were confirmed by X-ray photoelectron spectroscopy (XPS, XSAM 800, Kratos Ltd, UK) using Mg *K*α1,2 radiation, and data were processed by using Kratos Vision 2000. The overview spectra were taken between 200 and 1000 eV with an energy step of 0.5 eV using pass energy of 100 eV.

The interactions between QDs and matrix polymers were determined by Fourier transform infrared spectroscopy (FTIR, Nicolet 5700, Madison, WI) and fluorescence spectrophotometer (Hitachi F-7000, Japan). FTIR spectra of blank PGBELA nanoparticles and QDs-loaded nanoparticles were collected over the range of 4000–400 cm^{-1} using KBr pellets. The fluorescence spectra of free QDs in dichloromethane and QDs-loaded nanoparticles in water were measured using the excitation wavelength of 360 nm. The true-color fluorescent images of suspensions of QDs in dichloromethane and QDs-loaded nanoparticles in water were recorded with a digital camera under the radiation of an ultraviolet lamp (YX-450A, San-shen Medical Instrument Company, China).

Degradation Profiles of QDs-Loaded Nanoparticles Under Different pH Environment

The acid-labile characteristics of QDs-loaded PGBELA, PBELA and PELA nanoparticles were determined through the degradation tests with respect to the mass loss, molecular weight reduction and polydispersity changes. Briefly, preweighted nanoparticles were placed into 5.0 ml pH 7.4 and 6.0 phosphate buffer saline (PBS), and pH 5.0 acetate buffer solutions, which were kept in a thermostated shaking water bath that was maintained at 37 °C and 100 cycles/min. At predetermined intervals, triplicate samples were recovered, rinsed with distilled water to remove residual buffer salts, and dried to constant weight in a vacuum desiccator. The mass loss was determined gravimetrically by comparing the dry weight remaining at specific time with the initial weight. The dried nanoparticles were dissolved in tetrahydrofuran (THF, Thermo Fisher Scientific Inc., Fair Lawn, NJ), and the molecular weight of recovered polymers was determined by gel permeation chromatography (GPC, Waters 2695 and 2414, Milford, MA) with Styragel HT 4 column using polystyrene as standard.

Fluorescence Stability of QDs-Loaded Nanoparticles Under Different pH Environment

The emission intensities of QDs-loaded nanoparticles were determined after incubation into buffer solutions of different pH values. Briefly, QDs-loaded PGBELA, PBELA and PELA nanoparticles were placed into buffer solutions of pH 7.4, 6.0 and 5.0. The suspensions were exposed under continuous ultraviolet radiation and kept in a thermostated shaking water bath that was maintained at 37 °C and 100 cycles/min. At predetermined intervals, the fluorescence intensity of nanoparticle suspensions was measured by a fluorescence spectrophotometer with the excitation wavelength at 360 nm and emission wavelength at 450 nm.

Hemolysis Ability of Polymeric Nanoparticles Under Different pH Environment

The capability of PGBELA, PBELA and PELA nanoparticles to induce pH-dependent membrane destabilization was measured using hemolysis assay as described elsewhere (10). Briefly, whole human blood (Chengdu Blood Center, Chengdu, China) was centrifuged at 4 °C to obtain red blood cell (RBC) pellets, which were diluted with buffer solutions of pH 7.4, 6.0 and 5.0 to obtain cell suspension of 10^9 RBCs/ml. Then 100 μl of the RBC suspension was added into a 96-well tissue culture plate (TCP), followed by

adding 100 μl of nanoparticle suspensions of different concentrations from 0.2 to 2.0 mg/ml in each well, using pH 7.4 PBS and Triton X-100 (1.0 vol.%) as the negative and positive control, respectively. The microwell plate was incubated for 1 h at 37 °C, and then centrifuged at 2500 rpm for 10 min at 4 °C. The supernatant was collected and measured at 540 nm using μQuant microplate reader (Elx-800, Bio-Tek Instrument Inc., Winooski, VT). The results were expressed as percentage hemolysis with the assumption that Triton X-100 caused 100 % hemolysis and pH 7.4 PBS, no hemolysis.

In Vitro Cytotoxicity of QDs-Loaded Nanoparticles

HepG2 cells that over express asialoglycoprotein receptors and MCF-7 cells that have no galactose receptor were used in this study to determine the cellular uptake and distribution within cells of QDs-loaded nanoparticles. The cells were obtained from the American Type Culture Collection (Rockville, MD), and cultured in DMEM medium (Gibco BRL, Rockville, MD) supplemented with 10 % fetal calf serum (Gibco BRL, Rockville, MD). The cells were plated at 5000 cells/well in a 96-well TCP, and incubated for 24 h at 37 °C. Fresh media containing QD/PGBELA, QD/PBELA and QD/PELA nanoparticles with concentrations ranging from 6.0 to 24.0 μg/ml were added, using only media without nanoparticle as control. After 4 and 24 h intervals, MTT assay was performed, and the relative cell viability was calculated for each nanoparticle concentration compared with fresh media. To perform the assay, 20 μl of MTT stock solution (5 mg/ml in PBS) was added to the cells in each well and incubated for 4 h. Cell culture media was then removed and replaced with 100 μl dimethyl sulphoxide, and absorbance was read at 570 nm using a microplate reader as above.

Cellular Uptake Efficiency of QDs-Loaded Nanoparticles

The uptake efficiency of nanoparticles into cells was determined as described elsewhere (20). Briefly, after reaching 70–80 % confluency in 96-well TCP, HepG2 and MCF-7 cells were incubated with QD/PGBELA, QD/PBELA and QD/PELA nanoparticles at 1.0 nM QD concentration. In order to confirm that HepG2 cells can specifically recognize galactose residual via the asialoglycoprotein receptors located on their surface, 0.08 mol/l galactose solution was added to the cell suspension 30 min prior to the addition of QD/PGBELA nanoparticles (21). After incubation for 4 h at 37 °C, cells were washed three times with 100 μl PBS to remove unbound nanoparticles. Cells of each well were lysed by 50 μl 0.5 % Triton X-100 in 0.2 mol/l NaOH, and the fluorescence intensity was measured by a fluorescence spectrophotometer as above. Cellular uptake efficiency was expressed as the percentage of fluorescence intensity associated with the cells with respect to that presented in the nanoparticles added.

Subcellular Distribution of QDs-Loaded Nanoparticles

The targeting effect and capability of endosomal escape of QD/PGBELA nanoparticles were determined as described elsewhere with some modifications (22). Briefly, HepG2 cells were plated on microscope cover slides in a 24-well TCP, and cultured for 24 h. Cells were washed three times with PBS, and culture media containing QD/PGBELA and QD/PELA nanoparticles at the QD concentration of 1.0 nM were added. After incubation for 4 h, cells were washed three times with PBS, and then fixed with 2 % paraformaldehyde for 20 min. The cells were further washed three times with PBS and the endosome and lysosome were stained with LysoTracker Green DND-26 (Molecular Probes, Eugene, OR) for 30 min following the reagent instructions. Stained cells were washed three times with PBS and observed by confocal laser scanning microscope (CLSM, Olympus FV1000S, Japan) with the excitation wavelength at 405 nm for QDs observation and 504 nm for LysoTracker Green.

Statistical Analysis

The values were expressed as means ± standard deviation (SD). Whenever appropriate, two-tailed Student's *t*-test was used to discern the statistical difference between groups. A probability value (p) of less than 0.05 was considered to be statistically significant.

RESULTS AND DISCUSSION

Optimization of Preparation Process for QDs-Loaded Nanoparticles

Nanoprecipitation is a straightforward technique for the entrapment of drugs into nanoparticles with the size of 100–300 nm and high drug loading efficiency (23). In order to determine the effect of matrix polymers, QDs-loaded PGBELA, PBELA and PELA nanoparticles were prepared with close particle size and QDs loading amounts. The process parameters, such as the polymer concentration, the volume ratio of solvent and non-solvent, the amount of F68 used and the stirring rate were optimized. Table I summarizes the effect of process parameters on the particle size. An increase in the nanoparticle size was observed when the polymer concentration increased from 5 to 20 mg/ml

(batches 1–4). This phenomenon was related to the diffusion rate of the solvent towards the non-solvent phase. High viscosity of polymer solution showed a slow diffusion, leading to a large particle size. It should be mentioned that the formation of large aggregates was usually detected, resulting in a lower particle recovery for higher polymer concentration (results not shown). As shown in batches 5–7 of Table I, a decrease in the volume ratio of solvent to non-solvent from 1:5 to 1:25 led to decreased particle size from 300 to 210 nm. The lower ratio of solvent to non-solvent enhanced the precipitation of matrix polymers, leading to a decrease in the particle size (24). The use of surfactant could efficiently prevent the nanoparticle aggregation, and Guo *et al.* confirmed that QDs-loaded nanoparticles modified with F68 and sodium dodecyl sulfate lowered the cytotoxicity of QDs (19). Therefore, F68 was examined in the current study. As shown in Table I, no significant effect of the stirring rate (batches 2, 8 and 9) and the amount of F68 used (batches 2, 10 and 11) was found on the particle size.

Characterization of QDs-Loaded Nanoparticles

Table II summarizes the particle size, Zeta potential and QDs loading amounts of QD/PGBELA, QD/PBELA and QD/PELA nanoparticles. The obtained nanoparticles indicated diameters of around 200 nm, ensuring efficient cellular uptake (20). The Zeta potentials were around −20 mV, and the strong repellent forces among particles should prevent the aggregation of nanoparticles in buffer solutions (25). The QD loading amount of around 12 μg/g nanoparticles was designed to ensure only 1 QD was entrapped per nanoparticle on average, leading a minimal quenching inside nanoparticles. The yield and QDs encapsulation efficiency of PELA and PBELA nanoparticles were significantly higher than those of PGBELA nanoparticles. The hydrophilic groups of PGBELA caused higher affinity with the non-solvent of the nanoprecipitation system, resulting in drug leakage out of nanoparticles and less effective encapsulation during the nanoparticle formation. In the meantime, it is difficult to form particles completely in the non-solvent, leading to a low yield of PGBELA nanoparticles. As shown in Table II, the obtained PELA, PBELA and PGBELA nanoparticles indicated no significant difference in the particle size, Zeta potential and QDs loading amounts ($p>0.05$), which was essential to compare the acid lability and targeting capabilities of different matrix polymers.

Figure 1a and b shows the typical SEM and TEM morphologies of QD/PGBELA nanoparticles, indicating generally smooth surface and spherical shape with narrow size distribution. The particle sizes observed from SEM and TEM images were in good agreement with that determined by laser diffraction (Table II). Figure 1c shows XPS spectra of QD-loaded PBELA and PGBELA nanoparticles. There was no cadmium element present on the surface of nanoparticles, which proved that QDs were completely encapsulated inside the nanoparticles. A weak N1s peak at the binding energy of around 400 eV was presented on PGBELA nanoparticles, which confirmed the existence of galactose groups on the nanoparticle surface.

Figure 2a shows the emission spectra of the suspensions of free QDs in dichloromethane and QD/PGBELA nanoparticles in water at the same QD concentration, and the insets show the real object images under ultraviolet radiation. As indicated in the band edge emission at 420–480 nm, the full width at half maximum (FWHM) of free QDs and QDs in nanoparticles was around 20 nm, indicating a narrow size distribution. The trap-state emission at 500–700 nm of free QDs was ascribed to defect states at the surface of nanocrystals (26), while the intensity decreased significantly after entrapment into nanoparticles (Fig. 2a). The existence of matrix polymers made up for the sulfur vacancy and passivated the surface defects of QDs, thereafter enhanced the band edge emission and weakened the trap-state emission of QDs significantly. As shown in Fig. 2a, the emission peak of

Table I The Effect of the Nanoprecipitation Parameters on the Size of the Nanoparticles Obtained

Batch No.	Polymer Conc. (mg/ml)	S/NS ratio[a]	Stirring rate (rpm)	F68 content (%)	Particle size (nm)
1	5.0	1:10	400	5.0	160 ± 12
2	10.0	1:10	400	5.0	200 ± 16
3	15.0	1:10	400	5.0	320 ± 23
4	20.0	1:10	400	5.0	450 ± 29
5	10.0	1:5	400	5.0	300 ± 25
6	10.0	1:15	400	5.0	215 ± 18
7	10.0	1:25	400	5.0	210 ± 14
8	10.0	1:10	250	5.0	205 ± 22
9	10.0	1:10	600	5.0	185 ± 18
10	10.0	1:10	400	2.0	220 ± 24
11	10.0	1:10	400	10.0	202 ± 16

[a]Volume ratio of solvent/non-solvent

Table II The Characteristics of QDs-Loaded Nanoparticles

Nanoparticles[a]	Particle size (nm)	NFE (%)	Zeta-potential (mV)	EE (%)	AE ($\mu g/g$)
QD/PGBELA	210 ± 19	48.5 ± 3.1	−17.3 ± 1.3	37.8 ± 3.2	12.0 ± 1.2
QD/PBELA	195 ± 28	70.3 ± 6.7	−18.1 ± 1.7	63.1 ± 4.7	11.2 ± 1.0
QD/PELA	200 ± 32	66.4 ± 5.2	−22.1 ± 1.8	56.6 ± 4.3	11.6 ± 1.0

NFE nanoparticle formation efficiency; *EE* QDs encapsulation efficiency; *AE* the amount of QDs encapsulated

[a] PELA does not contain acetal nor galactose group, PBELA contains acetal groups only and PGBELA contains both

QDs in nanoparticles indicated a red-shift from 450 to 455 nm. This may be caused by the polarity change, resulting from the interactions with matrix polymers, and the slight change in the band gap energy of QDs (27). Another reason may be the decrease in the QD size during nanoparticle formulation. It was reported that sulfur atoms on the QD surface were oxidized by oxygen to form oxides, which would be desorbed from the surface (28). To determine the interactions between QDs and matrix polymers, FTIR analyses were performed on QD/PGBELA and blank PGBELA nanoparticles. As shown in Fig. 2b, a notable red-shift from 1700 to 1690 cm^{-1} was detected for the C=O bond of PGBELA after the introduction of QDs. The oxygen atoms of the matrix polymers formed Cd–O bands with excess cadmium atoms at the surface of CdS nanocrystals, thus making the vibration of C=O bond shift to lower wavenumbers.

Degradation Behaviors of QDs-Loaded Nanoparticles

Degradation profiles of QDs-loaded nanoparticles were assessed in buffer solutions of different pH values with respect to the mass loss, molecular weight reduction and the polydispersity changes of matrix polymers. Gravimetric evaluation of the mass loss during incubation is shown in Fig. 3a. There were about 4.9 %, 8.9 % and 9.8 % of mass loss for QD/PELA nanoparticles after incubation for 72 h in buffer solutions of pH 7.4, 6.0 and 5.0, respectively. There was less than 10 % of mass loss for QD/PGBELA and QD/PBELA nanoparticles after incubation in pH 7.4 PBS for 72 h. However, significantly higher mass loss was detected for above nanoparticles incubated in acid buffers. There were 25.2 % and 28.2 % of mass loss for QD/PBELA and QD/PGBELA nanoparticles after incubation in pH 5.0 buffers, respectively.

Figure 3b shows the molecular weight reduction of matrix polymers. Less than 10 % of M_w reduction was found for QD/PELA nanoparticles after incubation for 72 h in different buffer solutions. The molecular weight decreased gradually with incubation time, and significantly higher M_w reduction was indicated for QD/PBELA and QD/PGBELA nanoparticles after incubation in acidic buffer solutions compared with QD/PELA nanoparticles. Around 6.7 % and 7.6 % of M_w reduction were found for QD/PELA nanoparticles, and 24.3 % and 29.4 % for QD/PGBELA nanoparticles after incubation for 72 h in buffer solutions of pH 6.0 and 5.0, respectively.

As shown in Fig. 3c, an increase in the polydispersity was observed for all the nanoparticles. After incubation in pH 7.4, 6.0 and 5.0 buffer solutions for 72 h, QD/PELA nanoparticles showed about 3.0 %, 5.1 % and 6.5 % of increase in the polydispersity, respectively, which were close to those of QD/PBELA and QD/PGBELA nanoparticles after incubation in pH 7.4 PBS. However, there were around 15.0 % and 19.0 % of increase after incubation of QD/PBELA and QD/PGBELA nanoparticles in pH 5.0 buffer solutions for 72 h, respectively. The significant increase in the polydispersity may be caused by the breakdown of the acid-labile segments of ABA triblock backbone for matrix polymers PBELA and PGBELA.

From the results of mass loss, molecular weight reduction and the polydispersity increase, it was indicated that all the

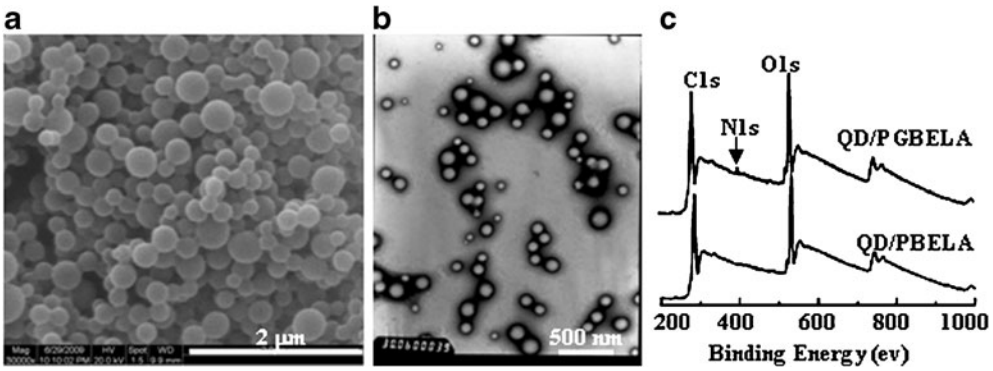

Fig. 1 SEM (**a**) and TEM images (**b**) of QD/PGBELA nanoparticles (**c**). C1s, N1s and O1s regions of XPS spectra of QD/PGBELA and QD/PBELA nanoparticles.

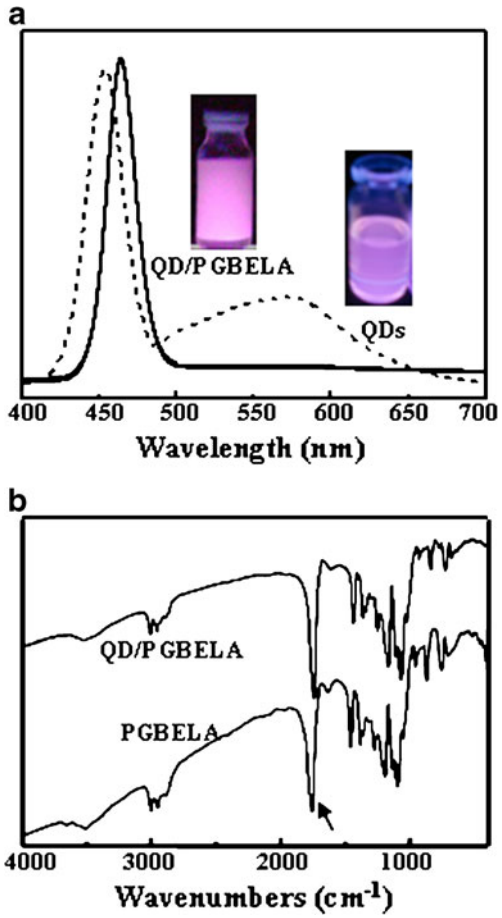

Fig. 2 (**a**) Fluorescence spectra of suspensions of free QDs in dichloromethane (*dotted line*) and QD/PGBELA nanoparticles in water (*solid line*) at the QDs concentration of 4.0 nM. Insets show the true-color fluorescent images recorded with a digital camera under ultraviolet radiation (**b**). FTIR spectra of PGBELA and QD/PGBELA nanoparticles. The *arrow* shows the absorption peak of C=O bond of PGBELA.

nanoparticles showed similar degradation behaviors in pH 7.4 PBS. But the degradation was enhanced for PBELA and PGBELA nanoparticles under acid conditions, indicating excellent acid-labile properties. In addition, due to the hydrophilic galactose grafts of PGBLEA, a slightly higher degradation rate was observed for PGBELA than PBELA nanoparticles.

Emission Stability of QDs-Loaded Nanoparticles

The breakdown of matrix polymers should affect the emission stability of QDs, which is another strategy to clarify the acid-lability of QDs-loaded nanoparticles. Figure 4a shows the emission intensities of suspensions of free QDs and QDs-loaded nanoparticles in buffer solutions of different pH values, ranging from 7.4 to 5.0, under continuous ultraviolet irradiation. As shown in Fig. 4a, there was no more emission of free QDs after ultraviolet irradiation for 45 min in buffer solutions of pH 5.0. The reduction in the emission intensity for free QDs may be mostly caused by the decomposition of QDs through radical reactions of oxygen under ultraviolet irradiation (29). In addition, QDs were synthesized in hydrophobic organic solvents, and easily aggregated together in aqueous buffers, which caused the fluorescence resonance energy transfer (FRET) (30). Moreover, when free QDs were exposed to acidic buffers, the surplus cadmium ions or sulfur ions on the QD surface absorbed other ions, such as protons or carboxylic acid ions by physical interactions, and the changes in the surface state eventually caused the fluorescence quenching (31).

The fluorescence quenching of QDs in acid buffers under continuous ultraviolet irradiation was used to determine the pH sensibility of matrix polymers. Figure 4b–d shows the relative emission intensities of QD/PELA, QD/PBELA and QD/PBELA nanoparticles after ultraviolet irradiation in different buffer solutions. QDs-loaded nanoparticles indicated higher emission stability after incubation in pH 7.4 PBS than free QDs, due to the protection effect of the polymer layer. A slight increase in the emission intensity was indicated after incubation for 4 h, which was probably caused by the photo-induced annealing of the surface defects of QDs (32). This indicated that the nanoparticle formulation of QDs had great advantages *versus* free QDs in increasing their fluorescent intensity as well as their photostability, which thus improved the image quality and extend their life-time for imaging.

As shown in Fig. 4, there was around 60 % of emission intensity retention after 24 h irradiation of QD/PELA nanoparticles in pH 7.4 PBS. However, the fluorescence emission reduced by a half and almost to zero for QD/PBELA and QD/PGBELA nanoparticles in buffer solutions of pH 6.0 and 5.0. The degradation of matrix polymers under acid conditions caused the leakage of QDs to the buffer solutions, leading significantly higher decrease in the emission intensity. The above results revealed that QD/PBELA and QD/PGBELA nanoparticles were significantly degraded in acid buffers, and relatively stable in neutral buffers.

Hemolysis Ability of Polymeric Nanoparticles

The disruptive activity of endosomal membrane of the acid-labile nanoparticles was evaluated using RBCs as the biological model membrane. Lysis of RBCs, i.e. hemolysis, has been shown to be predictive of a potential membrane disruption and is therefore a suitable preliminary test to determine the endosomal membrane disrupting activity (33). Figure 5 shows the hemolysis profiles of PELA, PBELA and PGBELA nanoparticles at different pH values, ranging from 7.4 to 5.0, and the selected pH values are based on the pH values in endosome (34). As shown in Fig. 5a, all the nanoparticles presented a similar and less than 5 %

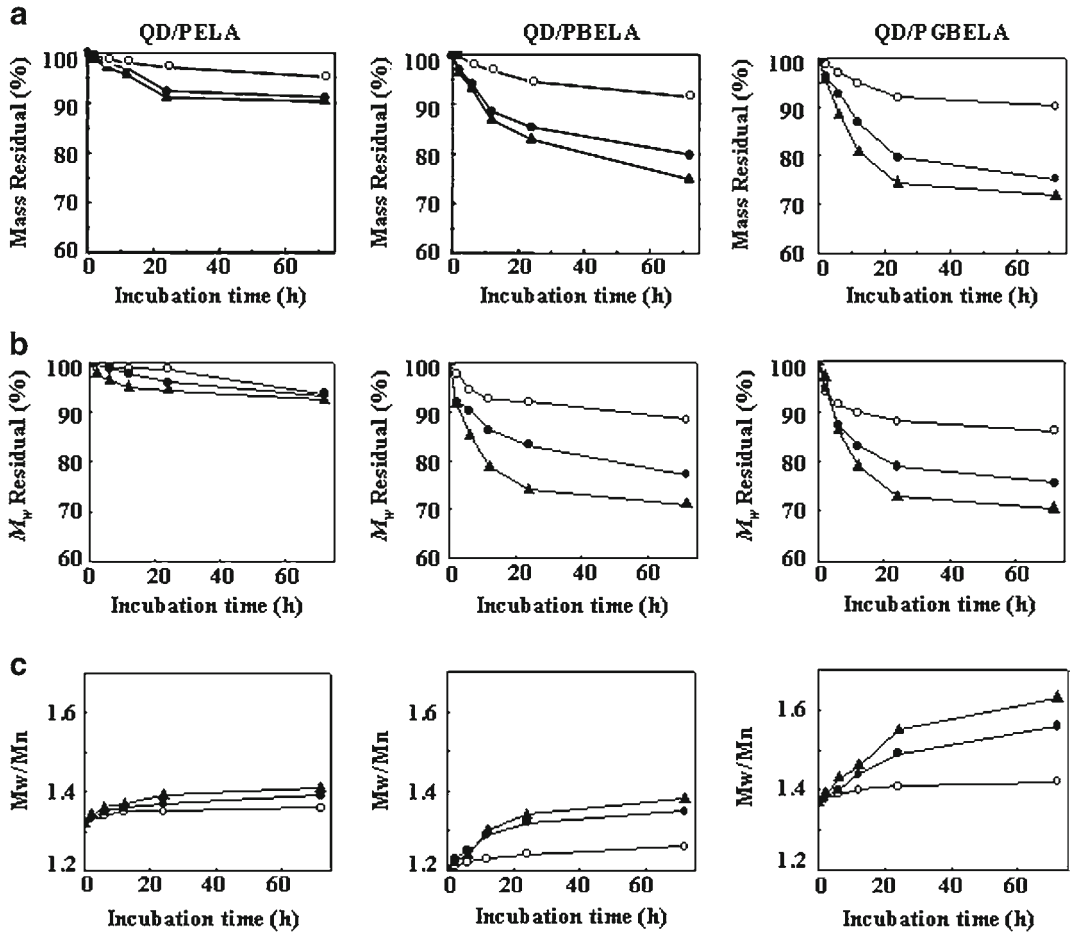

Fig. 3 The mass residual (**a**), molecular weight reduction (**b**) and molecular weight polydispersity increase (**c**) of QD/PELA, QD/PBELA and QD/PGBELA nanoparticles after incubation in buffer solutions of pH 7.4 (○), 6.0 (●) and 5.0 (▲) at 37 °C (n=3).

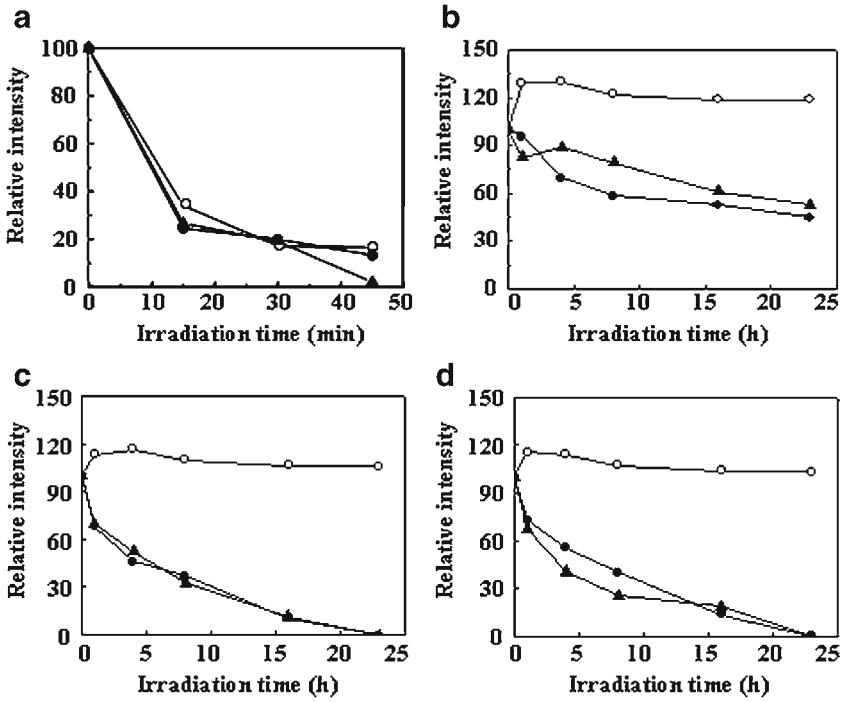

Fig. 4 The emission intensities of suspensions of free QDs (**a**), QD/PELA (**b**), QD/PBELA (**c**) and QD/PGBELA nanoparticles (**d**) in buffer solutions of pH 7.4 (○), 6.0 (●) and 5.0 (▲) after incubation at 37 °C under continuous ultraviolet irradiation (n=3).

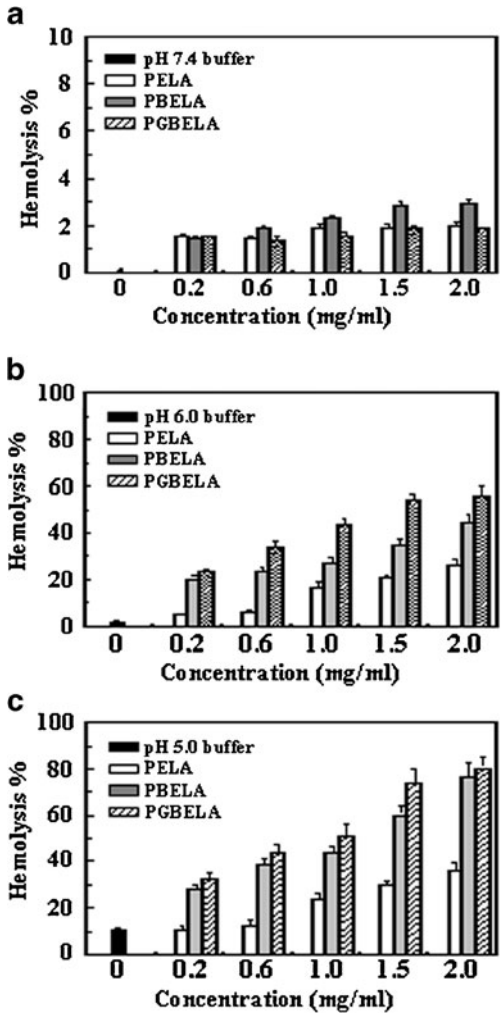

Fig. 5 Hemolysis capabilities of PELA, PBELA and PGBELA nanoparticles after incubation in buffer solutions of pH 7.4 (**a**), 6.0 (**b**) and 5.0 (**c**) ($n=5$). Hemolysis was normalized relative to that observed from the positive control, 1.0 % (*v/v*) Triton X-100.

hemolysis rate at pH 7.4 under different nanoparticle concentrations, ranging from 0 to 2.0 mg/ml. Significantly higher hemolytic activity was determined after incubation polymeric nanoparticles in acid buffer solutions ($p<0.05$), and the hemolysis gradually increased with increasing of the nanoparticle concentration. The hemolysis rates were up to 44 % and 56 % for PBELA and PGBELA nanoparticles, respectively, after incubation into pH 6.0 PBS at the concentration of 2.0 mg/ml, while significantly less hemolysis of 26 % was found for PELA nanoparticles due to the lack of acid-labile segments ($p<0.05$). When the pH value further decreased to 5.0, 78 % and 80 % hemolysis were detected for PBELA and PGBELA nanoparticles, respectively, which were significantly different from PELA nanoparticles with 36 % hemolysis at the same concentration ($p<0.05$). It should be mentioned that the acidic buffers also had a slight hemolytic activity, when the pH values decreasing from 7.4 to 5.0, the hemolysis increased up to 10 %.

The above results indicated that PBELA and PGBELA had good pH-dependent membrane disruptive activity, and may be best-suited for intracellular delivery applications (35). They were capable of disrupting endosomal membrane at an acidic pH, which should allow for safe release of trapped contents into cytoplasm, without destabilization of cell membranes at the physiological pH of 7.4. The hemolysis may be caused through osmotic mechanism (36). The degradation of matrix polymers resulted in oligomers and small molecular solutes, leading to an osmotic imbalance that caused RBC lysis. The higher hemolytic activity of PGBELA than PBELA nanoparticles can be attributed to the increase in the hydrophilicity of galactose graft on the acid-labile segments, leading to faster matrix degradation after incubation in acid environment.

In Vitro Cytotoxicity of QDs-Loaded Nanoparticles

The stable fluorescence of QDs makes it easy to follow in terms of signal during cellular uptake and subcellular location of nanoparticles, but indicate potential toxicity to cells and organism (37). So the toxicity of QDs-loaded nanoparticles was evaluated to optimize the dose of nanoparticles for the uptake and intracellular distribution study. It should be noted that free QDs could not be well dispersed in the cell culture medium and the cytotoxicity and uptake capability were not estimated. The nanoparticles containing 0.5, 1.0 and 2.0 nM of QDs was dosed based on previous study (14), and Fig. 6 shows the viability of HepG2 and MCF-7 cells after incubated for 4 and 24 h. The viability of HepG2 and MCF-7 cells decreased with the increase in nanoparticle concentrations from 6.0 to 24.0 μg/ml. There was over 80 % of cell viability when incubated with nanoparticles of 12.0 μg/ml, which was used in the following tests on the cellular uptake efficiency and subcellular distribution of QDs-loaded nanoparticles. It should be mentioned that a wide range of nanoparticle concentrations could be applicable for nanoparticles with entrapped other bioactive substances.

As shown in Fig. 6, there was no significant difference in the cell viability between the incubation time of 4 h and 24 h for MCF-7 cancer cells ($p>0.05$). The relative viability of HepG2 cells after incubation with QD/PGBELA nanoparticles was around 61.2 %, which was significantly lower than that with MCF-7 cells after 4 h incubation ($p<0.05$). Moreover, the cytotoxicity of QD/PGBELA nanoparticles was higher than that of QD/PELA and QD/PBELA nanoparticles after incubation with HepG2 cells for 24 h. The cell viability was around 82.5 %, 76.6 % and 58.4 % for QD/PGBELA nanoparticles with QDs concentrations of 0.5, 1.0 and 2.0 nM, respectively, which were significantly lower than 92.7 %, 90.1 % and 79.3 % for QD/PBELA nanoparticles at each QDs concentration ($p<0.05$). This may be attributed to the targeting effect of galactose moieties, resulting in higher uptake efficiency of PGBELA nanoparticles into HepG2 cells.

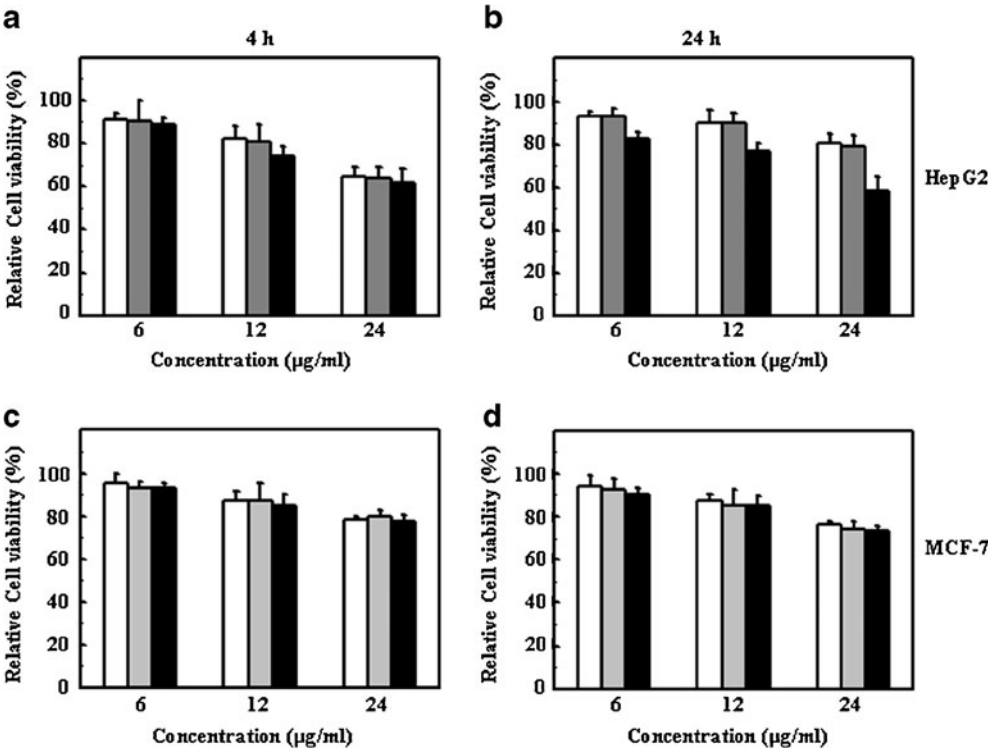

Fig. 6 The cytotoxicity of QD/PELA (*white column*), QD/PBELA (*grey column*) and QD/PGBELA nanoparticles (*black column*) of different concentrations after incubation with HepG2 (**a** and **b**) and MCF-7 cells (**c** and **d**) for 4 (**a** and **c**) and 24 h (**b** and **d**) ($n=5$).

This was also confirmed from the results of MCF-7 cells without asialoglycoprotein receptor, indicating no significant difference among QD/PELA, QD/PBELA and QD/PGBELA nanoparticles at each concentration ($p>0.05$).

Cellular Uptake Efficiency of QDs-Loaded Nanoparticles

To evaluate the targeting effect of QD/PGBELA nanoparticles, the cellular uptake efficiency was evaluated on MCF-7 and HepG2 cells, compared with QD/PELA and QD/PBELA nanoparticles. HepG2 cells have a high level of asialoglycoprotein receptors on their surface, and nanoparticles with surface modification by galactose groups become a potential strategy to enhance cellular uptake through receptor-mediated endocytosis (38). Figure 7 shows the cellular uptake efficiency after 4 h incubation with nanoparticles at the QDs concentration of 1.0 nM. There were around 24.5 %, 25.9 % and 26.8 % of cellular uptake after incubation QD/PELA, QD/PBELA and QD/PGBELA nanoparticles with MCF-7 cells, respectively, and no significant difference was found among the nanoparticles ($p>0.05$). Similar results were also obtained for QD/PELA and QD/PBELA nanoparticles after incubation with HepG2 cells. However, significantly higher cellular uptake efficiency of 51.7 % was detected for QD/PGBELA nanoparticles after incubation with HepG2 cells ($p<0.05$), which should be attributed to the galactose receptors. In order to confirm this assumption, excess of free galactose was added to the cell suspension 30 min prior to the addition of QD/PGBELA nanoparticles. As shown in Fig. 7, the uptake efficiency of HepG2 cells was significantly decreased to around 30.4 %, indicating the competitive binding of free galactose and galactose decorated nanoparticles with HepG2 cells, while there was no significant change for MCF cells. The results successfully confirmed that QD/PGBELA nanoparticles were taken up into HepG2 cells through the receptor-mediated endocytosis.

Subcellular Location of QDs-Loaded Nanoparticles

The location of QDs-loaded nanoparticles in subcellular compartments after endocytosis was evaluated by CLSM. Figure 8 shows images of HepG2 cells after incubation for

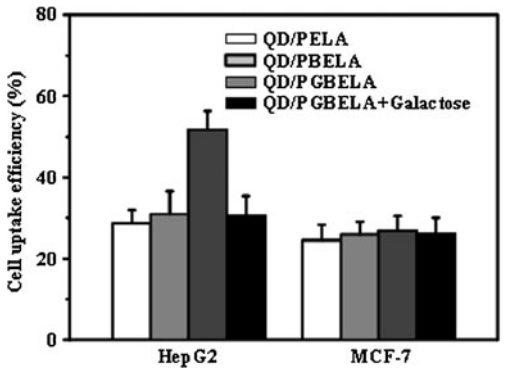

Fig. 7 The uptake efficiency of HepG2 and MCF-7 cells after incubation for 4 h with QD/PELA, QD/PBELA and QD/PGBELA nanoparticles. To test the galactose mediated targeting, 0.08 mol/l galactose solution was added to the cell suspension 30 min prior to the addition of QD/PGBELA nanoparticles ($n=5$).

4 h with QD/PELA and QD/PGBELA nanoparticles containing 1.0 nM of QDs concentration. Figure 8A reveals the uptake of QD/PGBELA nanoparticles and endosome staining of HepG2 cells. The images contained red fluorescence from QDs and green fluorescence from LysoTracker Green DND-26 for endosome. The representative images of a single cell after uptake of QD/PGBELA and QD/PELA nanoparticles are shown Fig. 8B and C, respectively. As shown in Fig. 8Bb and Cb, the fluorescence intensity of cells treated with QD/PGBELA nanoparticles was much higher than that of cells treated with QD/PELA nanoparticles, which was consistent with above results of cellular uptake. Co-localization of nanoparticles in endosome was observed as yellow from the overlap of green and red images. As shown in Fig. 8Dd and Cd, the nanoparticles were localized in the endosome after internalization. It should be noticed that QD/PELA nanoparticles were mainly located in endosome, while QD/PGBELA nanoparticles were not only located in endosome, also found in cytoplasm.

After uptake into cells, PGBELA matrix polymers reacted with protons in the endosome, and the proton consumption in acid organelles indicated a phenomenon similar to the proton-sponge effect, which caused the osmotic swelling due to an increased flux of protons and their counterions into the endosome. The buildup of osmotic pressure was able to destabilize the endosomal membrane and promote an endosomal escape (39). Moreover, as indicated in the hemolysis and degradation tests, the matrix polymers were degraded under acidic conditions and lots of oligomers were produced, which can also destabilize the endosome through osmotic mechanism and enhance the escape of QD/PGBELA nanoparticles into cytoplasm.

CONCLUSION

The cellular uptake, endosomal escape and subcellular distribution were clarified for acid-labile nanoparticles. The targeting effect of PGBELA nanoparticles were observed in the cytotoxicity test after nanoparticle treatment and the quantification of cellular uptake. The acid-labile characteristics led to an efficient escape of QDs-loaded nanoparticles into cytoplasm. The novel galactose decorated acid-labile biodegradable nanoparticles could provide efficient delivery not only to specific cells, but also to a variety of subcellular compartments and organelles. The above results indicate potential applications in *in vivo* labeling and imaging of cells and subcellular compartments utilizing QDs-loading nanoparticles which enhance fluorescence intensity. In addition, cytoplasm is the location for many biomacromolecules to

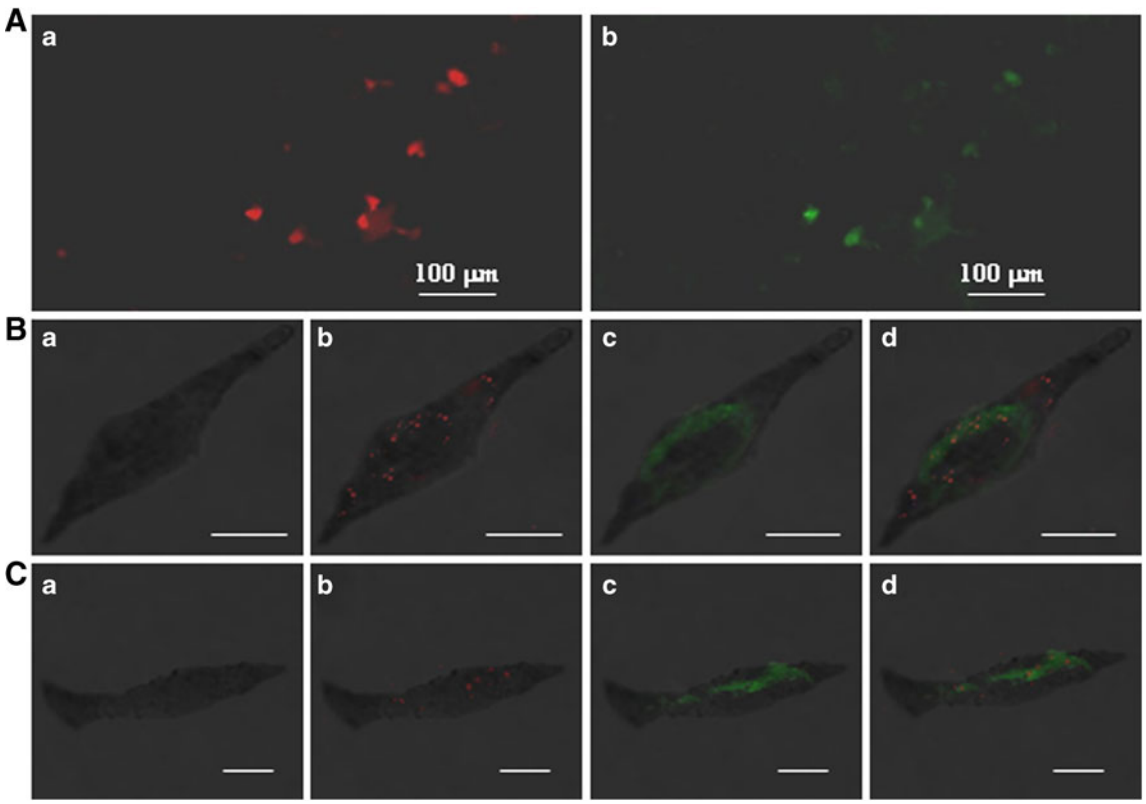

Fig. 8 (**A**) CLSM images of HepG2 cells after incubation QD/PGBELA nanoparticles (**a**) and endosome staining (**b**) Representative images of a single cell after uptake of QD/PGBELA (**B**) and QD/PELA nanoparticles (**C**): (**Ba** and **Ca**) transmittance images; (**Bb** and **Cb**) fluorescence images excited at 405 nm; (**Bc** and **Cc**) fluorescence images excited at 504 nm; (**Bd** and **Cd**) merged images excited at 405 and 504 nm. Scale bars represent 10 μm.

carry out their biological functions. Therefore, it is also suggested that galactose decorated acid-Labile nanoparticles can be expanded to incorporate bioactive substances, thereby providing a universal intracellular nanoscale delivery platform with significant potential in disease diagnosis, imaging and treatment.

ACKNOWLEDGMENTS & DISCLOSURES

This work was supported by National Natural Science Foundation of China (30570501, 20774075, and 51073130), and Fundamental Research Funds for the Central Universities (SWJTU11CX126 and SWJTU11ZT10).

REFERENCES

1. Wiethoff CM, Middaugh CR. Barriers to nonviral gene delivery. J Pharm Sci. 2003;92:203–17.
2. Pack DW, Hoffman AS, Pun S, Stayton PS. Design and development of polymers for gene delivery. Nat Rev Drug Discov. 2005;4:581–93.
3. Murthy N, Campbell J, Fausto N, Hoffman AS, Stayton PS. Bioinspired pH-responsive polymers for the intracellular delivery of biomolecular drugs. Bioconjug Chem. 2003;14:412–9.
4. Berg K, Selbo PK, Prasmickaite L, Tjelle TE, Sandvig K, Moan J, *et al*. Photochemical internalization: a novel technology for delivery of macromolecules into cytosol. Cancer Res. 1999;59:1180–3.
5. Mellman I. Endocytosis and molecular sorting. Annu Rev Cell Dev Biol. 1996;12:575–625.
6. Ding CX, Gu JX, Qu XZ, Yang ZZ. Preparation of multifunctional drug carrier for tumor-specific uptake and enhanced intracellular delivery through the conjugation of weak acid labile linker. Bioconjug Chem. 2009;20:1163–70.
7. Lo CL, Huang CK, Lin KM, Hsiue GH. Mixed micelles formed from graft and diblock copolymers for application in intracellular drug delivery. Biomaterials. 2007;28:1225–35.
8. Garripelli VK, Kim JK, Namgung R, Kim WJ, Repka MA, Jo S. A novel thermosensitive polymer with pH-dependent degradation for drug delivery. Acta Biomater. 2010;6:477–85.
9. Guo X, Szoka FC. Steric stabilization of fusogenic liposomes by a low-pH sensitive PEG-diortho ester-lipid conjugate. Bioconjug Chem. 2001;12:291–300.
10. Chen Z, Cai XJ, Yang Y, Wu GN, Liu YW, Chen F, *et al*. Promoted transfection efficiency of pDNA polyplexes-loaded biodegradable microparticles containing acid-labile segments and galactose grafts. Pharm Res. 2012;29:471–82.
11. Goto Y, Matsuno R, Konno T, Takai M, Ishihara K. Artificial cell membrane-covered nanoparticles embedding quantum dots as stable and highly sensitive fluorescence bioimaging probes. Biomacromolecules. 2008;9:3252–7.
12. Su YY, Hu M, Fan CH, He Y, Li QN, Li WX, *et al*. The cytotoxicity of CdTe quantum dots and the relative contributions from released cadmium ions and nanoparticle properties. Biomaterials. 2010;31:4829–34.
13. Delehanty JB, Mattoussi H, Medintz IL. Delivering quantum dots into cells: strategies, progress and remaining issues. Anal Bioanal Chem. 2009;393:1091–105.
14. Pan J, Feng SS. Targeting and imaging cancer cells by folate-decorated, quantum dots (QDs) loaded nanoparticles of biodegradable polymers. Biomaterials. 2009;30:1176–83.
15. Li H, Shih WH, Shih WY, Chen LY, Tseng SJ, Tang SC. Transfection of aqueous CdS quantum dots using polyethylenimine. Nanotechnology. 2008;19:475101–8.
16. Cui WG, Qi MB, Li XH, Huang SZ, Zhou SB, Weng J. Electrospun fbers of acid-labile biodegradable polymers with acetal groups as potential drug carriers. Int J Pharm. 2008;361:47–55.
17. Deng XM, Li XH, Yuan ML, Xiong CD, Huang ZT, Jia WX, *et al*. Optimization of preparative parameters for poly-DL-lactide-poly(ethylene glycol) microspheres with entrapped Vibrio cholera antigens. J Control Release. 1999;58:123–31.
18. Yu G, Li XH, Cai XJ, Cui WG, Zhou SB, Weng J. The photoluminescence enhancement of electrospun poly (ethylene oxide) fibers with CdS and polyaniline inoculations. Acta Mater. 2008;56:5775–82.
19. Guo GN, Liu W, Liang JG, Xu HB, He ZK, Yang XL. Preparation and characterization of novel CdSe quantum dots modified with poly(D, L-lactide) nanoparticles. Mater Lett. 2006;60:2565–8.
20. Win KY, Feng SS. Effects of particle size and surface coating on cellular uptake of polymeric nanoparticles for oral delivery of anticancer drugs. Biomaterials. 2005;26:2713–22.
21. Setua S, Menon D, Asok A, Nair S, Koyakutty M. Folate receptor targeted, rare-earth oxide nanocrystals for bi-modal fluorescence and magnetic imaging of cancer cells. Biomaterials. 2010;31:714–29.
22. Nam HY, Kwon SM, Chung H, Lee SY, Kwon SH, Jeon H, *et al*. Cellular uptake mechanism and intracellular fate of hydrophobically modified glycol chitosan nanoparticles. J Control Release. 2009;135:259–67.
23. Barichello JM, Morishita M, Takayama K, Nagai T. Encapsulation of hydrophilic and lipophilic drugs in PLGA nanoparticles by the nanoprecipitation method. Drug Dev Ind Pharm. 1999;25:471–6.
24. Gorner T, Gref R, Michenot D, Sommer F, Tran MN, Dellacherie E. Lidocaine-loaded biodegradable nanospheres. I. Optimization of the drug incorporation into the polymer matrix. J Control Release. 1999;57:259–68.
25. Mu L, Feng SS. Vitamin E TPGS used as emulsifier in the solvent evaporation/extraction technique for fabrication of polymeric nanospheres for controlled release of paclitaxel (Taxol®). J Control Release. 2002;80:129–44.
26. Ramsden JJ, Webber SE, Graetzel M. Luminescence of colloidal cadmium sulfide particles in acetonitrile and acetonitrile/water mixtures. J Phys Chem. 1985;89:2740–3.
27. Guo GN, Liu W, Liang JG, He ZK, Xu HB, Yang XL. Probing the cytotoxicity of CdSe quantum dots with surface modification. Mater Lett. 2007;61:1641–4.
28. Alivisatos AP. Perspectives on the physical chemistry of semiconductor nanocrystals. J Phys Chem. 1996;100:13226–39.
29. Hezinger AFE, Teßmar J, Gopferich A. Polymer coating of quantum dots—a powerful tool toward diagnostics and sensorics. Eur J Pharm Biopharm. 2008;68:138–52.
30. Li MJ, Zhang JH, Zhang H, Liu YF, Wang CL, Xu X, *et al*. Electrospinning: a facile method to disperse fluorescent quantum dots in nanofibers without Forster resonance energy transfer. Adv Funct Mater. 2007;17:3650–6.
31. Fan CH, Wang S, Hong JW, Bazan GC, Plaxco KW, Heeger AJ. Beyond superquenching hyper-efficient energy transfer from conjugated polymers to gold nanoparticles. Proc Natl Acad Sci USA. 2003;100:6297–301.
32. Yordanov G, Simeonova M, Alexandrova R, Yoshimura H, Dushkin C. Quantum dots tagged poly(alkycyanoacrylate) nanoparticles intended for bioimaging applications. Colloids Surf A. 2009;339:199–205.
33. Plank C, Oberhauser B, Mechtler K, Koch C, Wagner E. The influence of endosome-disruptive peptides on gene transfer using

synthetic virus like gene transfer systems. J Biol Chem. 1994; 269:12918–24.
34. Lee RJ, Wang SS, Low PS. Measurement of endosome pH following folate receptor-mediated endocytosis. Biochim Biophys Acta. 1996;1312:237–42.
35. Murthy N, Campbell J, Fausto N, Hoffman AS, Stayton PS. Design and synthesis of pH-responsive polymeric carriers that target uptake and enhance the intracellular delivery of oligonucleotides. J Control Release. 2003;89:365–74.
36. Tosteson MT, Holmes SJ, Razin M, Tosteson DC. Melittin lysis of red blood cells. J Membr Biol. 1985;87:35–44.
37. Fan TWM, Teh SJ, Hinton DE, Higashi RM. Selenium biotransformations into proteinaceous forms by foodweb organisms of selenium-laden drainage waters in California. Aquat Toxicol. 2002;57:65–84.
38. Popielarski SR, Hu-Lieskovan S, French SW, Triche TJ, Davis ME. A nanoparticle-based model delivery system to guide the rational design of gene delivery to the liver. 2. *In vitro* and *in vivo* uptake results. Bioconjugate Chem. 2005;16:1071–80.
39. Akinc A, Thomas M, Klibanov AM, Langer R. Exploring polymethylenimine-mediated DNA transfection and the proton sponge hypothesis. J Gene Med. 2004;7:657–63.